Turbine Design Report

2024 Collegiate Wind Competition

April 18, 2024

WIND POWER
CAL POLY, SAN LUIS OBISPO, CA

California Polytechnic State University, San Luis Obispo

Team Lead:
Trevor Ortega – tdortega@calpoly.edu

Team Manager:
Nora Riedinger – nrieding@calpoly.edu

Club Advisor:
Andrew Kean – akean@calpoly.edu

Turbine Design Officers:

Structures: Clayton Lahodny – clahodny@calpoly.edu

Blades: Ella Blaney – egblaney@calpoly.edu

Power: Keegan Leonard – kleona07@calpoly.edu

Structures Team:
Dillon Nelson
Sonny Quinday
Izik Hingeley
Andrew Cervantes
Sierra Bindseil
Nico Stallone

Blades Team:
Olivia Hoffsis
Cody Firman
Samuel Rothstein

Power Team:
Connor Hurban
Noah Fouts
Ryan Rayos
Luke Oliver
Joel Manesh
Alex Liu
Kalel Gadduang
Indigo Garcia
Dustin Wong
Hailey Ybarra
Timothy Chu
Lani Nguyen

Table of Contents

1. Design Overview

1.1 Executive Summary

Cal Poly Wind Power designed, built, and tested a small-scale wind turbine to compete in the 2024 Collegiate Wind Competition. Development of our 2024 turbine focused on growing from our experience as a learn-along team in 2023. The turbine rotor is a 3-blade variable pitch horizontal-axis design consisting of SD2030 primary airfoils with modified root and tip geometry capable of producing twice as much power as in 2023. The blades are manufactured using fused filament PLA and attach to the pitching mechanism with an internal spar. Testing has shown that they can withstand at least up to 3 times the normal operating rotational speed. An off-the-shelf ODrive D6374 150kV brushless DC motor will be used as our generator. Modeling and testing show a 30% improvement in our power score over the 2023 generator. The 3-phase AC output is rectified using low loss Schottky diodes. An Uno Rev3 microcontroller monitors turbine state, generates PWM signals for the pitching mechanism's linear actuators, and sets the variable load. Sensors and output devices are optically isolated as appropriate in accordance with the rules. A steel tower and foundation anchor the turbine to the sand tank. The foundation uses a hybrid suction screw relying on a combination of the sand's weight and suction effect to provide strength. Compared to the 2023 foundation, we were able to reduce the weight by 65% without reducing reliability.

1.2 Design Objectives

Turbine performance requirements were established in the fall to meet a goal of 230/300 points in the turbine testing competition: sustaining an extreme durability load case, 90% reliability in testing, having two systems capable of slowing the turbine by 90% in less than 10 seconds, keeping speed within +/-5% of setpoint during the control task, producing a power curve score of at least 30 points, keeping foundation weight under 3.5 kg, and supporting expected foundation loads at 98% confidence. The extreme durability load case was defined as a partial control system failure preventing the blades from feathering or the load from changing at 22 m/s. We have met or exceeded all these goals except efficiency, which has seen a maximum of 29.0 points. We also met our overall goal, scoring 237/300 points in a testing practice run.

1.3 Application of Previous Designs

Our team was a learn-along team last year, so we had a functional turbine that we were able to draw upon for the design of the 2024 turbine. Most components saw revision to meet our updated design goals, but a few systems remained the same. The hub and swashplate of our pitching mechanism were both designed to be used for multiple years and easily met our raised load requirements. This allowed us to maintain more quickly begin testing the new control system. The foundation follows the same conceptual design as last year, with reductions in the metal thickness used for weight savings. The vertical adjustment mechanism features the same dimensions as it continues to work with updated turbine parameters. Our electrical system still uses a BLDC motor and passive rectifier; however, the motor and rectifier are both different models from last year. We are currently using a controllable load set to a constant resistance, but an MPPT algorithm may be working reliably enough in time to be used at the competition.

2. Turbine Design Details

2.1 Combined Systems Model

New for this year, we have developed a comprehensive Simulink model which fuses static aerodynamic data from QBlade with dynamic models of the turbine mechanical, power, and control systems [1]. This was developed to allow for analysis of the turbine's dynamic response during the control and safety tasks but has the added benefit of simulating static operating conditions during the power curve and durability tasks. The model is also highly parametric, allowing us to compare new blades, generators, control systems, rectifiers, actuators, pitching mechanisms, and bearings. We first simulated the 2023 turbine and found the model correctly predicted performance to within 4% of actual behavior measured at the competition. Once the model had been validated, we then used it to guide design choices throughout the 2024 turbine. Details of how exactly the model was used for specific subsystems are discussed further where relevant.
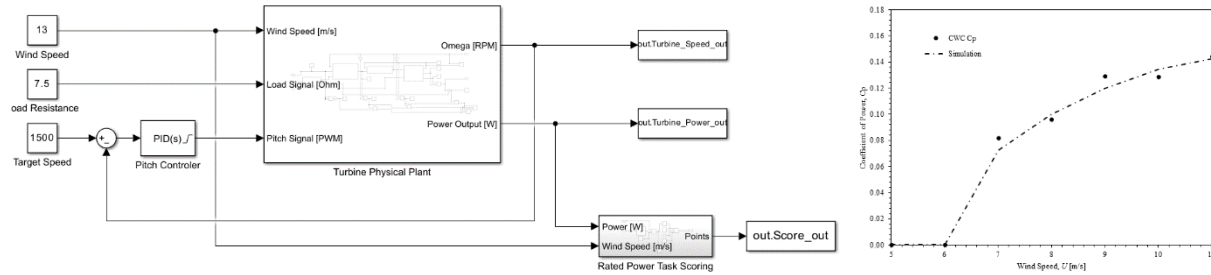

Figure 1. Schematic of Simulink model and plot showing agreement between simulation and 2023 testing.

2.2 Blade Design

2.2.1 Blade Aerodynamics

The design objective for the blades is to maximize power extraction from the wind based on the competition's power production weighting for 5-11 m/s wind speeds. This year, we set a goal of obtaining a power score of 30/50 according to the weighting mentioned. Major constraints were optimizing our blades for high RPMs and efficiency while also producing the torque needed to cut-in at 5m/s with our chosen generator. We found that a cut-in torque of 70 N-mm was required based on testing of the generator and comparison to blade models.

In comparison with the NACA4412 airfoil we used last year, our selected SD2030 main airfoil produces a higher cut-in torque at a given chord scale (CS) and TSR. This allows the turbine

Figure 2. 3D slice of blade torque space at 0 pitch.

to operate at all given wind speeds while also having a higher designed TSR, increasing power production significantly. Other airfoils, like the S1221 and GOE79, were considered, but it was found that the trailing edge was too thin to retain its shape during testing. Additionally, due to both airfoils' high degree of camber paired with our turbine's fixed pitch during the power task, there were concerns regarding the large amount of drag the airfoils would create at higher wind speeds.

All blade designs considered were created using our club's custom Blade Element Momentum Theory (BEMT) code, providing a base chord and twist for 25 elements of a given airfoil approximated at a Reynolds number of 68000, the mid-point for most of our blades. All blades were designed at a length of 19 cm to ensure they would fit with our hub within the 45 cm diameter. After creating a base blade, we applied chord scaling and variable Reynold's numbers in QBlade to measure power output, cut-in torque,
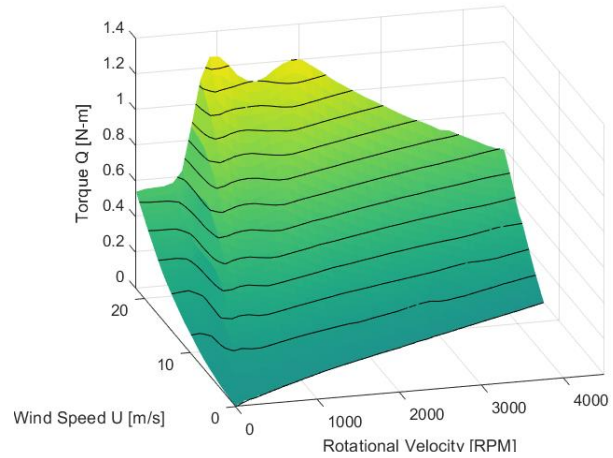
optimal pitch, and the optimal RPM at competition-specified wind speeds. This process was kept largely the same as last year but designed to operate at a higher TSR. QBlade's Schmidt Optimization method was considered in addition to BEMT during blade design, but it created blades with thinner overall chords and did not produce nearly as much power when scaled to the thickness necessary for cutting-in at 5 m/s. This year, we also considered our generator's RPM-related efficiency curve, obtained by our club's custom Simulink turbine model, while producing a simulated power score for each modeled blade. Our final blades have a designed TSR of 3.6 and a chord scale of 1.75.
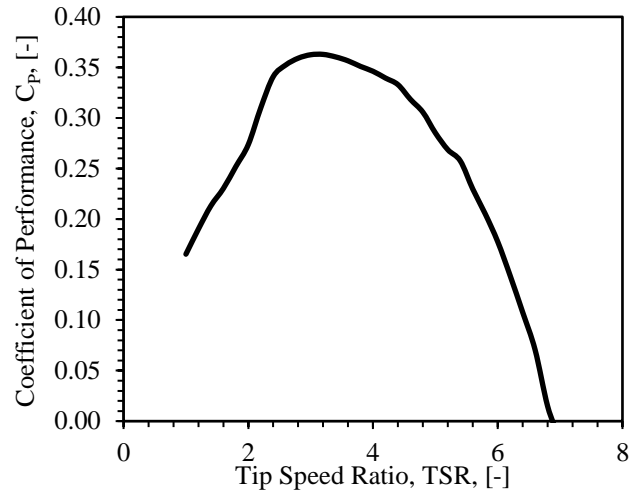

Figure 3. Theoretical Cp Lambda curve from QBlade.

Root and tip airfoils were incorporated into our blade design to account for structural stability and drag from tip vortices. Due to our blades thickness, structural stability was not a large concern for us, but a root airfoil, the SD7080 was used as it increased the QBlade-simulated power made by the blade. The MH 30, a thinner airfoil, was chosen for the tip of the blade for the purpose of reducing tip vortices. As with the SD7080, we verified in QBlade that it would increase our power score. The number of root and tip airfoils was also determined via QBlade analysis, and whole blades were validated experimentally in the wind tunnel. These airfoils, along with the main SD2030 airfoil are shown in Figure 4.
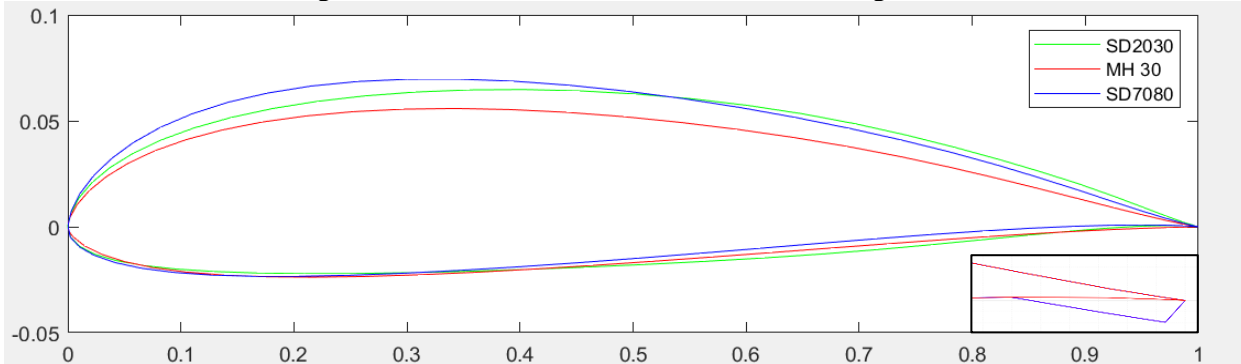

Figure 4. Root, Tip, and Main Airfoil showing the SD7080, MH 30, and SD2030 respectively. The inlay shows the modified trailing edge at a 2:1 scale.

2.2.2 Blade Manufacturing Process

The blades are 3D printed with PLA, using a 15% infill and a variable wall thickness that decreases towards the tip of the blade to reduce weight. Different post-manufacturing processes were tested in the wind tunnel, including surface smoothing using Isopropyl Alcohol and Poly Smooth PLA, as well as sanding our PLA blades. Both reduced output power, with the ISA smoothed blades performing 50% worse than identical unsmoothed blades.

One difficulty we ran into when manufacturing turbine blades was the uniformity of the blade's trailing edge. Our 3D printer has a minimum nozzle diameter of 0.4 mm, which conflicts with the airfoils' infinitely thin trailing edge. To print the trailing edge, the blades were modified so that the trailing edge of the airfoils were no thinner than 0.4 mm, as shown in blue in the Figure 4 inlay. This method of converting .dat files to 3D models allows the printer to print the trailing edge in one continuous pass, retaining the minimum thickness possible while avoiding the creation of gaps, print errors, and otherwise unreliable trailing edges.

2.2.3 Nosecone Design

The nosecone directs un-utilized airflow from our hub towards the blades. The geometry is a scaled version of GE's experimental EcoROTOR in Tehachapi Wind Farm [2]. The nosecone is attached to our turbine via an M3 hex-head bolt, which also constrains the pitching mechanism axially. In addition to a 4% power improvement recorded, it also improved cut-in torque. We also experimented with the distance forward from the hub, finding that it increased the power most when 5mm away.

2.2.4 Blade Testing Process

After being simulated in QBlade and manufactured with our club's 3D printer, we test the durability of blades before placing them in our university's wind tunnel. First, static testing is done by attaching our blades to a blade spar and clamping a wooden jig containing them to a table. We then use weights to apply an out-of-plane moment to the blades in the direction of loading from the wind, taking note of flexure and other signs of decreased performance or potential failure. With a thinner blade we designed, we tested the maximum moment able to be withstood and saw failure with a safety factor of 3.8 with respect to expected worst-case loading in QBlade, not to mention significant deflection beforehand. In addition to static testing, we also attached the turbine to a car to test the durability of our blades while facing the axial forces it would experience in the wind tunnel, along with a thrust-driven moment. We were able to spin the blades up to 4500 RPM using this method while observing only minimal signs of wear, if any. This was more than we expected to see during testing and sufficiently demonstrated the strength of our blades.

Blades' power output was also tested in our university's wind tunnel, in addition to validation of our nosecone, nacelle cover, blade post-processing methods, and control system response described later. Optimal generator resistance, pitch, and cut-in tests were also conducted there along with calculations of our power score for each new set-up. All told we spent over 50 hours in the lab, and the turbine ran for nearly 10 hours. The conclusion of this optimization is the turbine power curve shown in Figure 5.

There were concerns that the measured power output within our wind tunnel may be inaccurate due to blockage effects as it is only 2'x2' [3] [4]. However, when testing identical blades in Cal Maritime's 4'x4' wind tunnel, the average difference was only 7% with no directional bias. Based on this data we assume that blockage in our tunnel isn't significant enough to justify correcting for it within our analysis.

2.2.5 Annual Expected Power Output

Our turbine's annual expected power was calculated based on a wind distribution modeled after the CWC power curve scoring distribution. We felt this was a more reasonable data set than using the project development data as the power curve task represents the turbine's designed operating conditions and roughly follows a Weibull distribution. Across these wind speeds, the turbine would be producing a weighted average of 7.6 watts. Maintained over a year, this would produce a total of 66.6 kWhr. Across this range, the turbine has an average overall coefficient of power of 0.277. Losses in this condition are distributed fairly evenly, with the electrical system operating at 76% efficiency, and the blades running at 62% of the Betz limit.
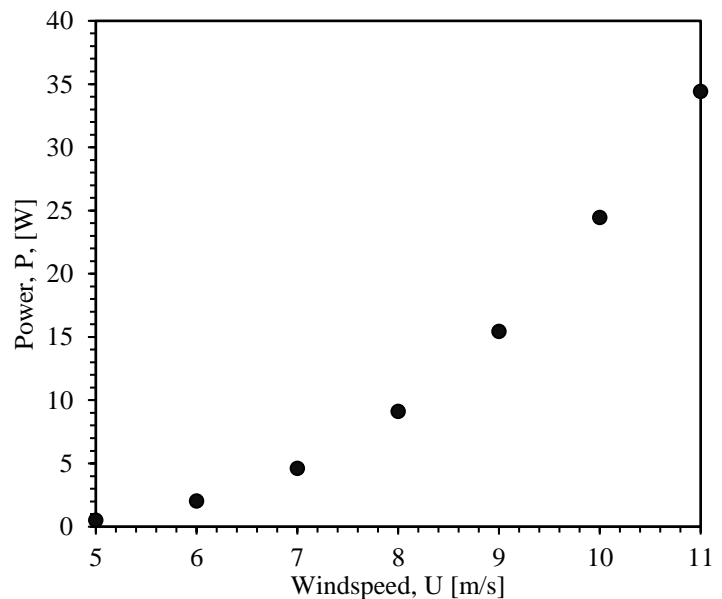

Figure 5. Final power curve testing results corresponding to a score of 29 points.

2.3 Mechanical Load Analysis

2.3.1 Blade and Spar Structural Design

In addition to design requirements related to aerodynamic performance for the power task, the blades and rotor must also meet our durability goals. Structural components must be resilient enough not to fail even in the event of a nonfunctional control system. At the 2023 competition, our turbine only partially feathered during the durability task, causing extremely high loading. Our Simulink model indicated that the turbine could have reached a speed of 6300 RPM if feathering had fully failed. Loads in this case are primarily due to a centripetal force of 1.8 kN, with minor contribution from aerodynamic thrust and torque. The Simulink model was also used to evaluate loads during all operating and braking conditions, but this case was by far the most severe. Because this load case is outside of typical operating conditions and we can inspect components for yielding after such an event, we are designing for a safety factor of 1.0.

The pitching mechanism and blades are attached to the shaft using a stack-up consisting of a bolt through the blade, bonded spar, hub cap, bearing, bolt in the root, and hub. This configuration was developed last year, but changes were made to the spar and hub to allow for a wider range of safe operating conditions and better clearances for lower friction. The pitching motion is driven by two linear actuators through a swashplate and three linkage arms. The hub transmits torque through a D flat machined in the shaft. A section view of CAD, FEA, and the final mechanism are shown in Figure 6.

Figure 6. Section of blade spar stack, FEA study of loads in the spar, and photo of finished assembly.

Analysis of the strength of the blade attachment began with manual stress calculations to identify areas of concern before FEA was used in critical locations to verify the accuracy of our hand calculations. Stresses at both bolts, the spar, the bearing, and the threading in the hub were analyzed. The weakest point in the system is where the 3D-printed blade is attached to the hub. The internal metal spar avoids interrupting the aerodynamic exterior of the blade and transmits bending and twisting loads well; however, centripetal force is only carried by an M3 bolt loaded in shear. The bolt itself is a high-strength alloy steel, but bearing and tearout stress in the surrounding PLA are of greater concern. The initial plan was for the spars to be machined from 7075 aluminum, but we found that it did not have enough strength to balance the competing interests of blade and spar strength without increasing the size of the base airfoil. Instead, the spar is separated into two parts bonded with high-strength Loctite 638 and a press fit steel pin. Areas of high stress are made of Ti 6Al-4V while the rest remains aluminum, allowing it to be manufactured on manual mills and lathes without requiring CNC operations as was done last year. With this arrangement, the blade has a safety factor of 1.1, and the titanium spar has a safety factor of 1.1 at the bolt hole and 2 at the bonded joint. A blade spar and body without the pin were used as test coupons, and we verified that the adhesive exceeded its rating by 10%.

Once we had updated blade designs for the 2024 turbine, we re-evaluated the turbine runaway condition in Simulink to ensure that our loads were still valid. We found that the new blades had a lower maximum expected speed at 4900 RPM which increases our minimum safety factor to 1.5. During testing, we forced a control system failure which matched the simulated load case and saw an actual maximum speed of 4500 RPM, a difference of less than 10%. The blades and spar were inspected afterwards, and no signs of yielding were found. Safety factors for this load case are shown in Table 1.

2.3.1 Mechanical Systems and Load Analysis

The rotor connects to the drivetrain from the D-flat on the driveshaft. The shaft is supported centrally by a bearing and rigidly coupled with the generator. The generator mount also holds the linear actuators for the pitching system, and a small 3D-printed mount in the rear to hold the encoder. A bronze bushing is pressed into the tower to yaw the nacelle, allowing the baseplate to rotate freely. To secure the nacelle's position, two tabs are bolted to the underside of the nacelle and clamp onto the bushing.
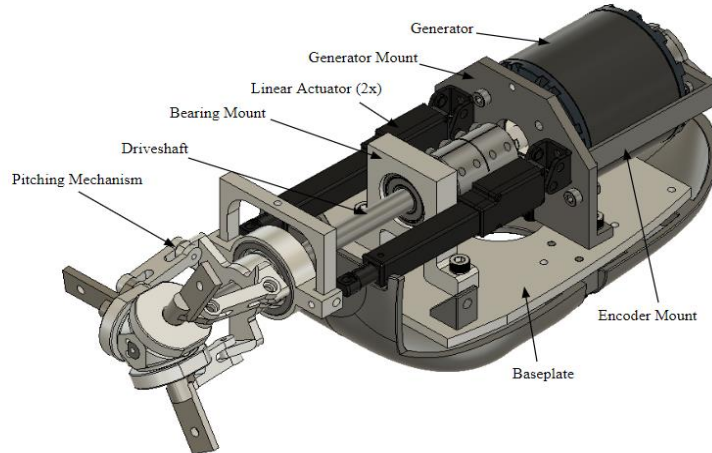

Figure 7. (Above) View of the yaw clamping lock on underside of nacelle plate.

(Left) Labeled view of the nacelle.

Load analysis was performed on the driveshaft, mounting, and tower. The axial loads considered were rotor thrust and wind drag. Radial forces from weight and rotational imbalance were accounted for. The rotor thrust was determined using the QBlade model for our worst case overspeed scenario. To allow for uncertainty in the model, a thrust of 30 N was used. The distributed load of the wind was calculated across the length of the cylindrical tower, reaching 14 N/m at 22 m/s.

The tower, in contrast to last year's aluminum model, is steel to increase stiffness and move our resonant frequency outside of our operating range. The calculated natural frequency of the turbine is about 2900 RPM. With a maximum operating speed of 1750 RPM, we expect the turbine to operate safely below resonance, and, in the case of runaway, the turbine will quickly pass through the resonance zone. The weld between the tower and the circular base has a factor of safety of 82.0 under the given loading. Similarly, all mounting components have large safety factors above 25. The driveshaft, using the Goodman criterion, has a factor of safety of 7.9 with 99% reliability [5].
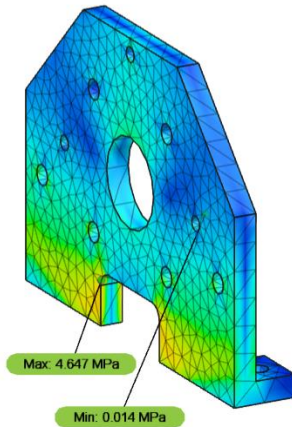
Table 1. Component strength calculations, most bolted connections are not listed as they generally have very large safety factors.

Part	Material	Stress (MPa)	FoS
Driveshaft	1566 Carbon Steel	24.7	7.9
Nacelle Plate	6061 Aluminum	1.7	140
Bearing Mount	6061 Aluminum	0.54	448
Generator Mount	6061 Aluminum	4.65	59.1
Tower-Flange Weld	ER70S-6 Filler	1.76	82.0
Spar Bonded Joint	Loctite 638	31	2.0
Spar Base	7075 Aluminum	199	2.5
Spar Hole	Ti 6Al-4V	315	1.6
Spar Tearout	Ti 6Al-4V	119	2.2
Blade Bolt	Class 12.9 Steel	290	3.3
Blade Tearout	Hatchbox PLA	24.5	1.9
Blade Shear Failure	Hatchbox PLA	12.0	2.0

2.3.2 Foundation Design and Load Analysis

This year's foundation follows the same conceptual design as last year's foundation, with changes made to reduce weight and meet our goal of 3.5 kg. The curved legs and angular feet twist into the sand using an installation bar bolted to the top cylinder. To account for the varying water level, two concentric cylinders are fit together, with the inner cylinder having threads, and the outer cylinder having matching slots such that bolts can clamp the inner part in place. This allows for 3 cm of total vertical adjustment, accounting for the 2 cm water level variation.
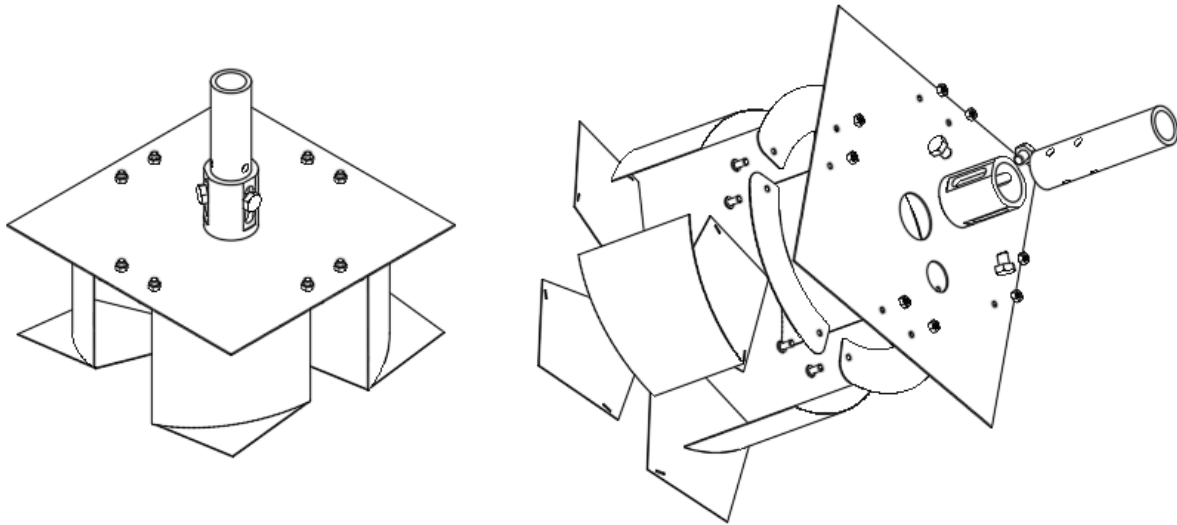

Figure 8. Isometric and exploded view of foundation assembly showing legs and adjustment mechanism.

The major concerns in this foundation design were functionality and weight. Last year's foundation was able to withstand turbine runaway at 17 m/s wind speed after the control system failed. This led to the reuse of the design. One observation from last year's foundation was that the thickness of the sheet metal used was large compared to the expected loading. The thickness of the top plate was highlighted for this issue, as last year's model used ¼" thick plating, which contributed to the 9.5 kg mass. The design goal for the updated foundation was to use significantly thinner sheet metal to accomplish the same result.
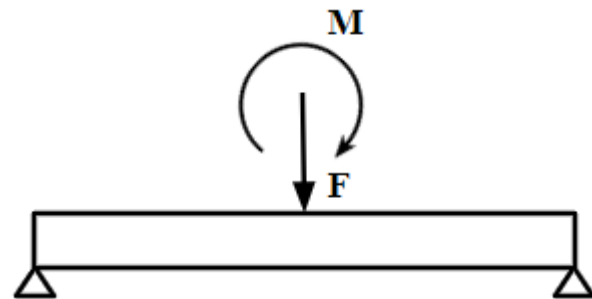

Figure 9. Schematic of loads used for foundation structural design.

Structural analysis of the top plate was performed using the model above. This model was used to determine the minimum allowable sheet metal thickness for turbine overspeed loads. This conservatively assumes all of the support comes from the legs, and none from the plate resting on the sand. Force **F** represents the weight of all components on top of the plate (tower, nacelle/rotor, tower, and transition stub), and moment **M** represents the overturning moment from wind drag and rotor thrust. 16-gauge steel sheet metal results in a safety factor of 2.1 for this model. This, along with thinner foundation legs, has decreased the mass of the foundation to 3.5 kg, meeting our team's goals for the Foundation Weight task. The weld between the plate and outer adjustment mechanism piece had a safety factor of 287.

$$Q_u = A'\left(q_c + q_q + q_\gamma\right) + PH_s\left(\frac{S_{ut}}{S_t} + \gamma_b z_{avg}\tan(\delta)\right)$$

Bearing capacity analysis of the sand was performed using the Handbook for Marine Geotechnical Engineering as a guide, the primary equation of which is shown above to calculate the bearing capacity Q_u [6]. This equation models a plate with an overturning moment and vertical force applied with the sand

providing distributed support. Because the foundation sits atop the sand, $H_s, q_q = 0$, and $q_c = 0$ because the sand is cohesionless. This leaves the effective area A' multiplied by the frictional bearing capacity q_γ. Initially, the safety factor of the bearing capacity of the sand was calculated to be less than 1 at runaway, but we decided to focus on empirical testing because we have found the foundation consistently outperforms the geotechnical model in the past due to ignoring suction effects and the geometry of the rotational legs under the sand. With those effects under consideration, the model was instead prototyped and tested. In each test, the foundation outlasted the goal overturning moment of 65 N-m, corresponding to runaway loading with a factor of safety of 2.0. Failures were seen at 72 ± 3 N-m.

2.4 Electrical System Design

  The electrical system is composed of 2 main parts – the control box and the load box. The control box includes the 3-phase rectifier, which connects from the AC generator, converts it to a DC, and then connects to multiple points: the point of common coupling (PCC), the voltage and current sensor, and the 5-volt buck-boost. The voltage and current sensor are connected to an Arduino Uno in the load box through an optocoupler. The control box buck-boost provides a constant 5-volt node for the pitch actuators and braking circuit activation. Between the boxes, the DC rectified cables will be measured by the PCC. Once in the load box, the buck-boost will regulate how much power will be consumed by the load resistor, creating a variable load. This variable load will be controlled by the Arduino Uno. The Arduino Uno is powered by an outlet from an outside source and will additionally govern the pitching, control state, and emergency stop states of the system.
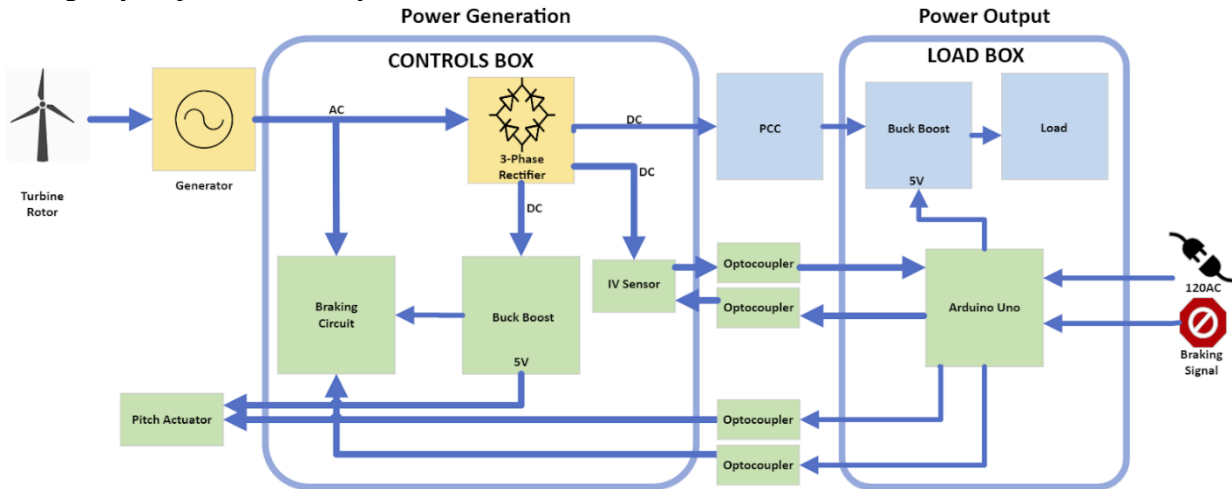

Figure 10. Diagram of electrical system showing the generator, rectifier, braking circuit, control buck boost, IV sensor, optocouplers, PCC, load buck boost, load, and Arduino Uno.

2.4.1 Generator

  A 3-phase 150kV BLDC ODrive D6374 motor was chosen for our generator. Multiple generators were simulated in Simulink, and this generator showed the best expected performance. This motor performs well because of its 150kV rating, which yields a greater voltage per RPM compared to the previous years' designs of 270kV. This higher voltage was also needed for components such as the buck boost that requires 2.8 volts to start. Higher voltage also decreases I^2R and diode losses.

2.4.2 Power Rectification

  In order to convert the 3-phase AC voltage produced by the generator, six fast recovery Schottky diodes and 5x1mF capacitors were placed in a bridge-rectifier circuit configuration. The diodes chosen have a forward voltage drop of 0.3 V, leading to a 0.6 V voltage drop across the circuit to minimize losses at the rectifier. The parallel 1 mF capacitors act as a low-pass filter, keeping our power ripple to less than 3%, safely within the specified 10% tolerance. Based on nameplate rating, they have a total energy storage capacity beneath the 10 J limit.

2.4.3 Optocouplers

The optocouplers are capable of sending signals between the load and control boxes while remaining electrically isolated. This allows us to ensure constant power to the Arduino Uno by placing it on the load side of the PCC. This allows us to monitor and control the turbine throughout the braking task. Optocouplers are ICs designed specifically for transmitting signals across electrical isolation with a signal transferred through light. To ensure the reliability of the optocouplers, we designed and printed the optocouplers on printed circuit boards. We have a second optocoupler board for use with the I2C protocol the Current and Voltage sensor uses to communicate with the Arduino. A schematic of the PCB created for the optocouplers is shown in Figure 11.
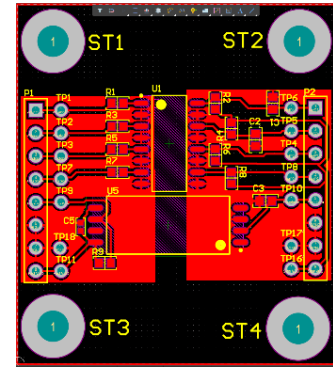

Figure 11. Optocoupler PCB.

2.4.4 Current, Voltage and Encoder

A closed-loop control system needs feedback in order to adapt properly. Our system uses an INA260 power sensor rated for up to 36 V and 15 A in series with the output of the rectifier to record voltage, current, and power. The other feedback source is a CUI AMT102-V capacitive encoder on the generator reading at 48PPR rated up to 7500 RPM. Both sensors report their information to the Arduino through the optocoupler system.

2.4.5 Control Buck Boost

To provide constant 5 V for our triac braking circuit and our actuators, a buck-boost was designed to provide a power bus with 5 V regardless of input voltage. This buck-boost activates at 2.8 V, which will be turned on before the wind tunnel reaches a wind speed of 5 m/s. We chose the robust low-power MP28167-A buck-boost module from Monolithic for its 2.8-22 V input range, configurable output voltage, and continuous output current rating of 3 A. This module has built-in OVP, OCP, overheating protection, and an optional internal control interface via I2C for changing characteristics such as switching frequency. This module additionally has a 95% efficiency at 1 A for 5 V.
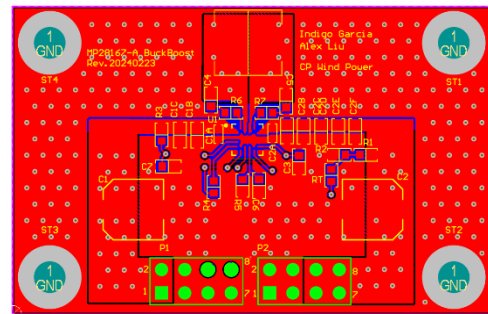

Figure 12. Control side buck boost PCB.

The datasheet provided a typical application circuit diagram for a 5 V output, which we used for all external components. This led to us designing our own PCB for this module, as shown in Figure 12. The I2C is optional, as it is not required to interface with it to change the output voltage. We did, however, design the PCB board to have 2 header pins for I2C interfacing in case it's needed.

2.4.6 Load Buck Boost

To optimize power generation, the effective load resistance must be variable to track the maximum power point of the wind turbine generator system. A 100 W capable reference design buck-boost converter with I2C interface was chosen to allow the Arduino microcontroller to programmatically continuously vary the load presented to the generator despite the physical load resistor being a fixed 1 Ω 100 W power resistor.

The buck-boost converter achieves this by changing the input-to-output voltage relationship. The converter's output regulation control loop will adjust its switching to maintain this output voltage as long as the input is within its limits. For example, with a fixed 1 Ω resistor, the load can be set to a power point of 25 W by setting the output voltage to 5 V. If the input voltage were 10 V, this would be the equivalent of having a resistive load of 4 Ω.

The Arduino changes the various registers in the buck-boost converter over I2C. These registers control the voltage output, internal reference voltage, internal feedback ratio, and other parameters. Since these registers can be configured by the Arduino, the buck-boost allows the load controller to adjust the power setpoint as demanded by any MPPT algorithm.

2.4.7 Braking Circuit

In order to ensure success in the emergency stop task, we have designed a solid-state triac-based braking system. The triacs are placed in parallel with each AC generator phase prior to the rectifier to maximize the amount of power they consume when activated. Once the triacs are given a gate signal from the Arduino, they short the 3 phases through 6.8 Ω resistors. This immediately increases the load of the turbine. This system is necessary to increase the load during the PCC disconnect task since we will not have access to the variable load. This triac braking system acts in conjunction with the Arduino, sending a PWM signal to the actuators that will feather the blades. The combination of feathered blades and triac load is enough to reduce the RPM by 90% within 10 seconds.

2.4.8 Cables

One focus of the team this year is a greater emphasis on organization. For our power cables, we have used color-coordinated silicon-coated wires that are very pliant. To reduce clutter in the control box and improve our assembly time, we implemented power and ground rails as a common node that components can connect to. For our signal cables, we used Cat7 ethernet cables to ensure organized individual signal isolation without any unwanted signal interference. We are using Anderson Powerpole connectors and an RJ45 ethernet connector at the base of our turbine, which historically has been the most time-consuming portion of the turbine installation process. Practice runs of the full installation process have generally taken 1:30, which is easily less than the allotted 3:00.
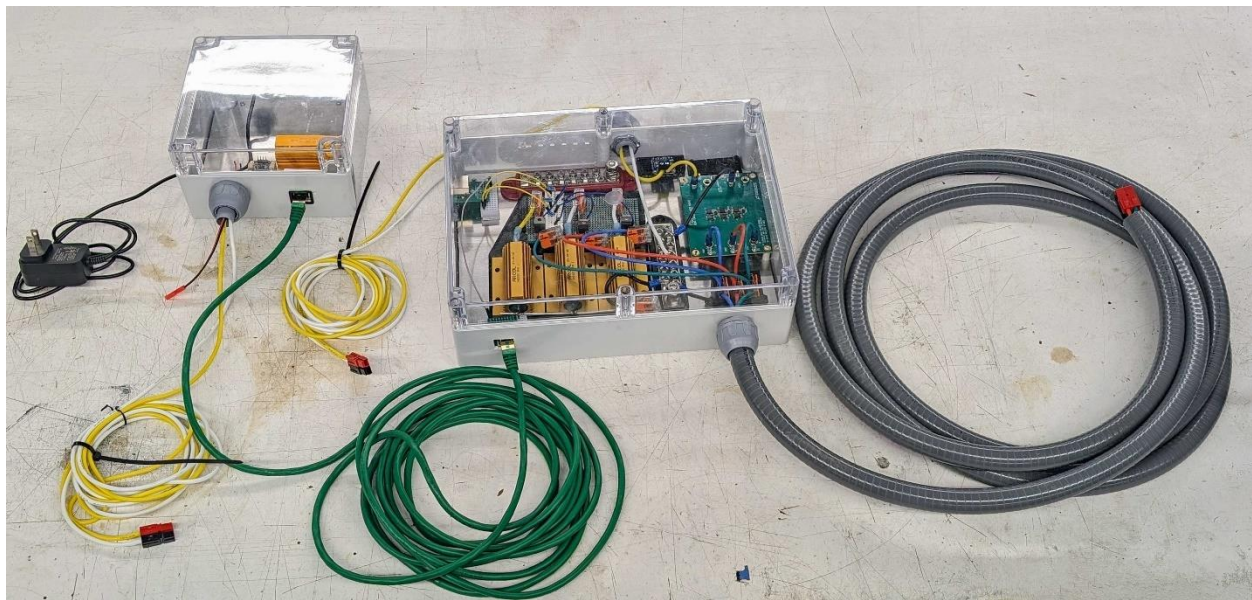

Figure 13. Photo of cabling and NEMA rated enclosures. The load is on the left and control is on the right.

2.5 Controls System Design

2.5.1 Control System States

The control system currently implemented was driven by the requirements for power regulation when above 11 m/s and braking during the safety task. We are targeting control within ±5% for 48 points and braking within 10 s as specified in the rules. The turbine uses a state system responsible for switching between startup, operational, and safety modes. During the startup mode, the blades are positioned to maximize cut-in torque and overcome cogging in the generator. Once above 300 RPM, the turbine switches to the operation state, maximizing turbine power until above a set RPM. Once above the set RPM and power, the blades begin feathering and the resistance is held constant to maintain a constant speed and power. When the safety shutoff state is triggered, the blades feather to brake the turbine and the generator is shorted to slow the rotor more quickly. A full depiction of our control system states as implemented in software is shown in Figure 14.

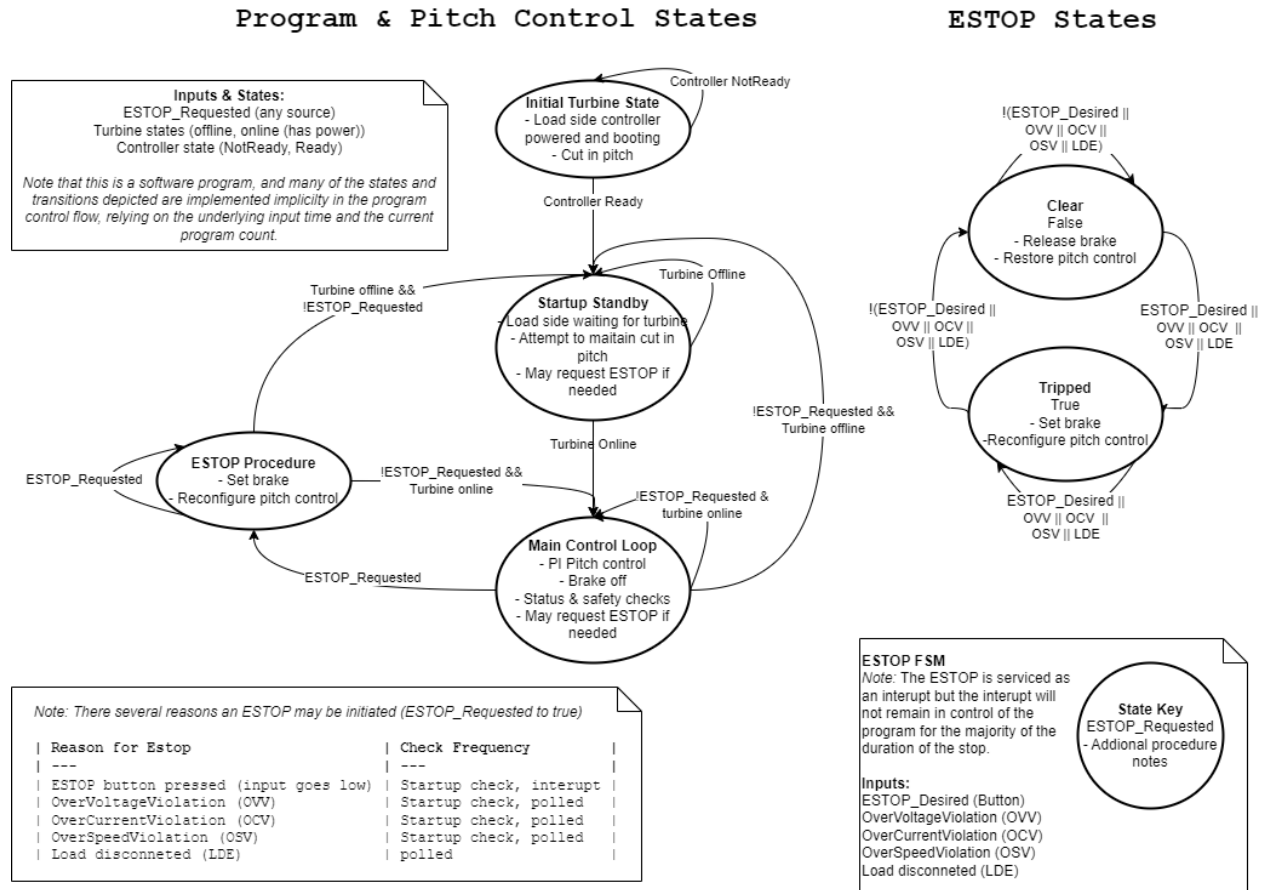## Program & Pitch Control States ESTOP States

Figure 14. Control State Diagram showing relationships between the Initial State, Startup Standby, Main Control Loop, and ESTOP. The ESTOP logic shows what conditions trigger and reset the ESTOP state.

During startup, the generator produces a cogging torque which must be overcome before the rotor will spin. Testing of our generator showed a cogging torque of 60-70 N-mm, which the blades must overcome before they cut in. To achieve this the blades are partially feathered to an angle of 24 degrees which we found produces the most reliable cut in.

The operation state is responsible for maintaining the blades at an optimal angle for power production from 5-11 m/s and then gradually feathering the blades to maintain a constant speed once above 11 m/s. A PI control feedback loop drives two Hi-Tec linear actuators attached to the turbine pitching linkage. During the power task the control setpoint for the PI loop is set to the rotor speed associated with 10.5 m/s as found during prior testing. At wind speeds beneath 11 m/s, the rotor speed will be less than the setpoint, and the pitch will be driven to a minimum angle of 13 degrees experimentally chosen to maximize power output. At 11 m/s and above, the rotor speed will be above the set-point and the angle will increase until the error is eliminated. This strategy was selected as it is robust to changes in turbine system parameters and does not require precise state estimation. An MPPT control algorithm for the load value has also been developed for the power curve task, but further testing is required to prove its reliability for use at competition. We estimate a further 3-point improvement in power output if implemented. The control loop currently implemented is shown in Figure 15 with an example target speed of 1500 RPM. Recent improvements in power output mean the setpoint used will be slightly higher.

For the braking state the same PI control loop is used, except the control setpoint is below 0 RPM. This immediately causes the blades to begin feathering until they reach the maximum angle of the pitching mechanism, which is set to produce the largest aerodynamic braking torque. The electric braking system is also triggered, as described in the electrical section.

2.5.2 Control System Physical Modeling

Design of the PI feedback loop was performed in Simulink using our turbine system model. Once the blades and generator had been selected based on power curve requirements, other parameters important to the control system response were the rotor inertia, linkage geometry, and actuator speed. We took measurements of our printed blades' inertia using a trifilar pendulum for use in the model. Our model predicted that fully stopping the turbine with pitch alone required increasing the range of our pitch by 43 degrees, so changes were made to the linkages to allow for this. Comparisons of the theoretical and actual kinematics of the mechanism were taken with an optical coordinate measuring machine. We found that the 2023 mechanism had about 3 degrees of backlash which negatively affected the system response when included in the control system model. The 2024 pitching mechanism, therefore, includes precision Teflon spacers, which successfully reduced backlash to 0.3 degrees. Based on the linkage geometry, our model indicated that the linear actuators needed a loaded speed of at least 1.3 mm/s and a stroke of 20 mm to be able to brake by 90% within 10 seconds. The specifications of the HLS12-50380 actuators used on the 2023 turbine met these requirements with testing showing a stroke speed of 2.9 mm/s, so they were selected for use on this year's turbine.
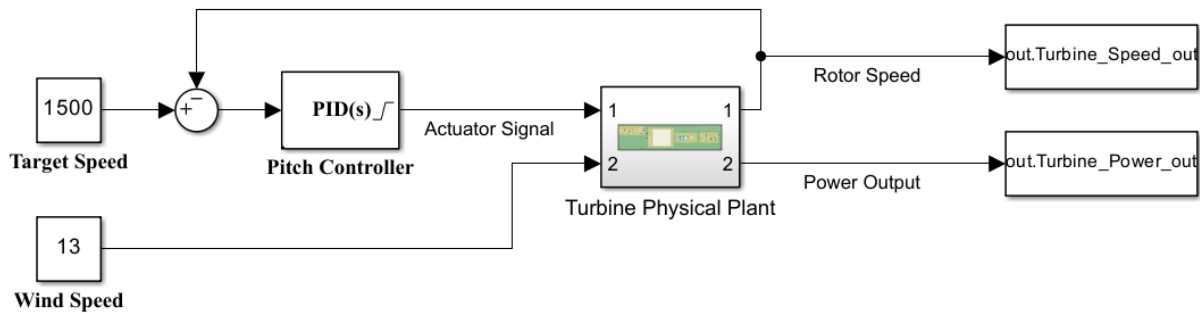

Figure 15. The Simulink model used to model the performance of the turbine control system. The actual turbine physical model is collapsed to a single block for clarity.

To evaluate the accuracy of the turbine dynamics model and assess the performance of the turbine control system, an input step response test was performed at 11 m/s. A comparison of the predicted response from Simulink is overlaid in Figure 16 with actual turbine data and bands representing our target score of 48/50 points. The turbine had a rise time of 10.4 s, a settling time of 16.8 s, and 24% overshoot. These parameters are all within 10% of their predicted values. The two points of instability visible are due to the actuator's position drifting very slowly through their backlash. Tests of wind speed steps and a braking signal were also within 10% of actual turbine performance results.
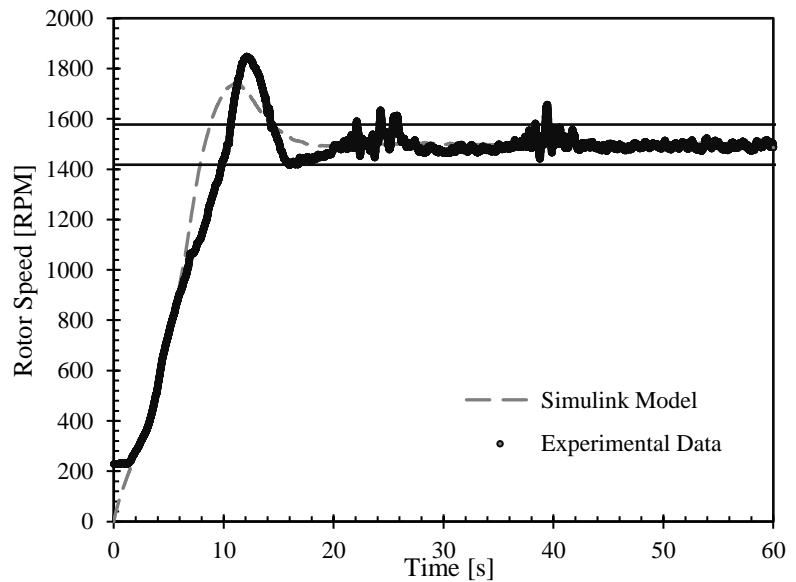

Figure 16. Comparison of model response and actual turbine response to turbine cut in and blade feathering.

2.5.3 Software Architecture and Development

Initially, we started writing a single file Arduino C++ program, but found it somewhat uncomfortable to work with as the file length increased. Eventually, it was refactored according to object-oriented principles (OOP). This made the main file clearer, encapsulated and abstracted the details of how various subsystems worked, and made the underlying custom libraries reusable. This came at the cost of a 2% increase in program size and memory usage, as well as requiring a slightly more thorough understanding of C++ to efficiently make changes. The increased difficulty of understanding the code has been mitigated with more thorough documentation than used in the past.

The program consists of a main file, a subsystem class for the pitch controller, and libraries for interfacing with hardware. The main file performs initialization procedures, facilitates high-level state control of the program, and manages the variable load. It also contains the utility method needed to interface with the emergency stop button, which is implemented as an interrupt. We also used an OEM-provided library to monitor our power sensor, an Adafruit INA260 breakout board.

Next, the pitch controller subsystem has its own class, as it is one of the most complicated parts. This includes its own initialization code and, state control, and consists of three objects: one for our specific pitch actuator, whose class itself is a customized wrapper for the Servo library, a singleton instance of our custom encoder class, and an instance of an open source PID library [7]. The pitch controller subsystem software was initially configured based on the Simulink models and was then tuned and verified with experimental data from wind tunnel tests. All parts of the code also use a custom log formatter and handler inspired by the Python logging module for improved debugging over generic print statements.

Due to the complexity of the project, additional tools were used in addition to Arduino IDE 2.0. The majority of the program was written using Microsoft Visual Studio Code and various extensions, such as SonarLint (code quality/static analysis). For revision control and backups, git and GitHub were selected. When supplemented with GitHub Actions, a cloud-supported automation and continuous integration/delivery/deployment (CI/CD) environment, this allowed for automated code verification, file size and memory usage reporting, and automated documentation generation with Doxygen.

3 Final Assembly

Since installation time is limited, as much as possible is assembled prior to our testing slot. The foundation legs will be fastened to the main foundation plate, and the adjustment tube will have the bolts installed but not tightened. The generator and bearing mount will be fastened to the baseplate and the shaft coupling will be tightened. The actuators and pitching mechanism will be secured with Loctite. After tests are performed to confirm functionality, the nacelle cover will be installed, and the yaw lock prepared. The turbine will then be ready for the timed installation. For a list of all fasteners used in non-permanent connections, see Table 2. The only fasteners that need to be secured during the time portion are two of the yaw lock bolts once the turbine is aligned and the wingnuts used to secure the turbine to the transition stub. Electrical connections that must be made during the timed slot are only those impossible to avoid: power and control at the top of the transition stub, our control box, the PCC, and the E-Stop. During practice, this process took less than half the allotted time. Distributed manufacturing was managed with 3 meetings a week which allowed officers to coordinate their designs. Compatibility with previous designs was maintained where possible to ease testing.

Joint	Fasteners	Qty
Foundation Legs	M6	8
Foundation Adjustment	M10	3
Nacelle Cover	M3	9
Yaw Lock	M4	4
Generator Mounting	M5	2
Generator	M4	4
Encoder	M2.5	2
Bearing Mount	M5	2
Actuator Mount	M5	2
Swashplate	M3	2
Pitching Linkages	M2.5	6
Blade Spar	M3	3

Table 2. List of turbine assembly fasteners

4 Commissioning Checklist

	Assembly Step	Perf.	Chkd.
Prior to Testing	Feed wiring through foundation and check continuity.		
	Attach foundation legs, adjustment tube, and installation bar.		
	Assemble components in nacelle, tightening all bolts as necessary.		
	Feed wiring down tower, place yaw locks, and check continuity.		
	Secure pitching mechanism to shaft and actuators.		
	Install blades on pitching mechanism and secure nacelle cover.		
	Verify electrical components in load and control boxes are secure.		
	Connect the turbine, control, and load boxes and run test program.		
	Upload competition program.		
25 Minute Install	Install foundation in the sand tank verifying level with bubble level.		
	Adjust stub height as necessary.		
	Remove foundation installation hardware.		
6 Minute Install	Connect control side AC wires and controls from foundation to control box.		
	Connect turbine side AC wires and controls from foundation to turbine.		
	Fasten turbine to transition stub, adjust yaw orientation, and lock yaw brake.		
	Connect isolated signal wires between load and controls.		
	Connect DC power cables from controls and load through the PCC.		
	Connect E-stop button to control box.		
	Connect load box to wall power and verify program startup.		

5 Final Testing

System tests were performed throughout the year to inform design decisions, verify models, and identify issues. After these were complete, we assessed our turbine's overall performance in a manner similar to the competition itself to evaluate whether we met our design goals.

5.1 Durability

The first category of tests was durability. This was assessed in two ways: testing for mechanical failure in an extreme load case and reliability assessment across all testing. For the extreme load case, the turbine was set to a blade angle and electrical load which matched our power curve position. The wind tunnel was ramped to 22 m/s and held for 30 seconds, allowing the turbine to reach a speed of 4500 RPM. The turbine was then removed and carefully inspected. We found no component failures and the turbine voltage remained within allowable operating limits. Assessing reliability is more difficult; we mainly focused on the frequency of component failures and malfunctions across our various tests. Early issues occurred frequently, but over time they significantly decreased as improvements were made. We have not had any component failures during the past few testing sessions at over 2 hours of continuous turbine operation without issues. If we treat this operating time as representing a sample of 24 successful durability tests and assume a binomial distribution, then we can calculate with 95% confidence that our failure rate is less than 1 in 10 durability tests.

5.2 Safety

The next set of tests are measurements of the ability to complete the braking task. For this test, the wind tunnel was set to various speeds and the E-stop was triggered. The RPM during this test was measured and we found that it dropped to under 10% within 5 s. The pitch and electrical brakes were tested separately and were both able to independently achieve successful braking within 10 s. A plot of a test of the E-stop taking place at 11 m/s is shown in Figure 17 with a line marking the 10% requirement.

5.3 Control

The control task was assessed based on our target criteria of RPM control within 5% above 11 m/s. With our fixed load, this should result in a score of 48/50 for this task. Better control results in only marginal gains, while the score quickly drops with larger error. The turbine was provided with bins of wind speed from 11-14 m/s and allowed to settle before proceeding to the next wind speed for testing. The turbine output was then compared to a previous measurement at 11 m/s and used to calculate a control ratio and associated score. This is shown in Figure 17, along with our 5% target band. The rotor speed ratio only exits this band during the steps in wind speed at 60, 100, and 130 seconds. The average error at each speed was 0.04%, -0.01%, -0.2%, and 0.3% for 11-14 m/s, respectively, but there is a steady state oscillation of ±2% with a period of 10 seconds present. We know this oscillation is due to actuator backlash, which we are hoping to eliminate with better tuning. Regardless, this performance already meets our design requirements, so the behavior is acceptable, and further tuning is not strictly necessary.
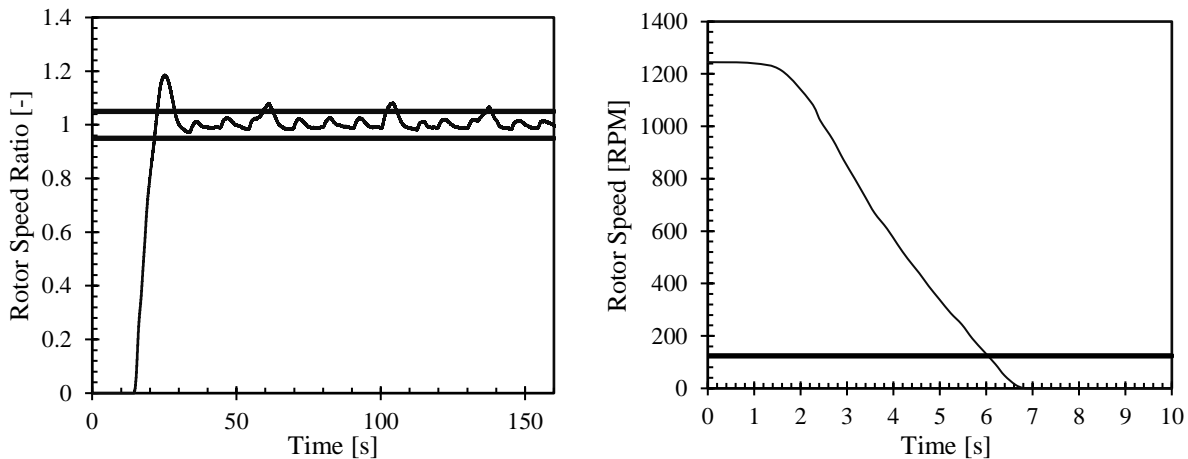

Figure 17. Plots showing control system response across 4 wind speed steps and braking task. Each time the turbine exists the target region during the control task is due to a 1 m/s step in wind speed.

5.4 Power Curve

The power curve score is the only requirement we have not met in testing yet, with our best power score of 29.0 falling just short of the desired 30 points. The power score data was collected at a fixed pitch and resistance without MPPT, since we are most confident we will be able to run this configuration reliably at the competition. An improved rectifier design with lower diode losses has functioned well in benchtop testing and once implemented should increase our score by 4.4 points, meeting our goal. This represents a doubling over our best results last year.

5.5 Foundation Success

We are not able to test our foundation directly with the turbine in our wind tunnel due to space limitations. Instead, expected results for the foundation success task were calculated by repeatedly installing the foundation in a sand and water tank and measuring the thrust required to displace the stub by 25 mm. 8 trials were conducted and we found a safety factor of 1.5 over expected loading with 98% confidence. Installation takes approximately 5 minutes, providing ample time to correct issues and adjust if needed.

5.6 Foundation Weight

Our goal of 3.5 kg for foundation weight was set based on an interpolation of foundations which we knew weights for from last year. Based on this interpolation we calculated that a foundation of this weight would score 25 points. The final foundation weighs 3.5 kg, exactly meeting our goal, but as we do not yet know the weight of our competitor's foundations, we cannot assess whether this will be light enough for our goal of 25 points in this category.

References

[1] K. Burnett, "A Proposed Control Solution for the Cal Poly Wind Energy Capture System," Cal Poly Mechanical Engineering Department, San Luis Obispo, 2012.

[2] T. Kellner, "Phys.org," 9 June 2015. [Online]. Available: https://phys.org/news/2015-06-ge-unveils-experimental-ecorotr-turbine.html.

[3] H. Ross and B. Polagye, "An experimental assessment of analytical blockage corrections for turbines," Department of Mechanical Engineering, University of Washington, Seattle, 2019.

[4] M. J. Werle, "Wind Turbine Wall-Blockage Performance Corrections," *Journal of Propulsion and Power,* vol. 26, no. 6, pp. 1317-1321, 2010.

[5] R. G. Budynas and J. K. Nisbett, Shigley's Mechanical Engineering Design, New York: McGraw-Hill Education, 2014.

[6] T. David and D. J. Beasley, "Handbook for Marine Geotechnical Engineering," Naval Facilities Engineering Command Engineering Service Center, Port Hueneme, 2012.

[7] B. Beauregard, "Improving the Beginner's PID," 15 April 2011. [Online]. Available: http://brettbeauregard.com/blog/2011/04/improving-the-beginners-pid-introduction/.